



TEM and PAS study of neutron irradiated VVER-type RPV steels

J. Kočík^{a,*}, E. Keilová^a, J. Čížek^b, I. Procházka^b

^a Division of integrity & Technical Engineering, Nuclear Research Institute Řež plc., 250 68 Řež near Prague, Czech Republic

^b Faculty of Mathematics and Physics, Department of Low-Temperature Physics, Charles University, V Holešovičkách 2, 180 00 Prague 8, Czech Republic

Received 26 September 2000; accepted 29 January 2002

Abstract

Conventional transmission electron microscopy and positron lifetime and Doppler broadening positron annihilation spectroscopy techniques have been used to investigate the radiation-induced microstructural changes in surveillance specimens of VVER-type reactor pressure vessel (RPV) steels, and RPV steels irradiated in the research reactor. Defects visible in transmission electron microscopy consist of black dots, dislocation loops and precipitates concentrated along the dislocation substructure. Their size and density depend on the neutron flux and fluence. The parallel set of thermally aged specimens, specimens recovery annealed after irradiation and specimens irradiated in a lower neutron flux was investigated too. No defects discernible in transmission electron microscopy were found after accelerated irradiation in the research reactor. In addition to visible defects, the small-volume vacancy clusters were identified by positron annihilation spectroscopy. © 2002 Elsevier Science B.V. All rights reserved.

1. Introduction

Neutron irradiation induces significant changes in both the microstructure and the properties of reactor pressure vessel (RPV) steels. These effects are attributed to the development of fine-scale radiation-induced defects in the crystal lattice of a material. Many sophisticated methods, each being selective to a specific part of the radiation-induced defect population, have been developed and employed to characterise radiation damage structures including atom probe field ion microscopy (APFIM), small angle neutron scattering (SANS), field emission gun scanning transmission electron microscopy (FEGSTEM), transmission electron microscopy (TEM), positron annihilation spectroscopy (PAS), anomalous small angle X-ray scattering (ASAXS), etc. [1]. In this

paper the TEM and PAS – including positron lifetime (PL) and Doppler broadening (DB) – techniques have been chosen to characterise microstructural changes in surveillance specimens of VVER-type RPV steels, and RPV steels irradiated in the research reactor.

Generally, the microstructural damage process proceeds in two steps:

- Formation of a high point defect concentration. Vacancies and self or solute interstitial atoms and their ultra-fine clusters are created during neutron induced displacement cascades processes. The energy dissipation within the cascade proceeds very quickly (<10 ns) and is only weakly dependent on the temperature [2–4].
- Defect microstructure evolution. New fine scale features are formed within a matrix by strongly temperature-dependent irradiation-enhanced diffusion processes, rearranging a primary point defect population created in cascade processes: the point defects can be removed from the matrix by recombination and annihilation, by trapping in sinks, or by coales-

* Corresponding author. Tel.: +420-2 6617 3223; fax: +420-2 2094 0519.

E-mail address: koc@ujv.cz (J. Kočík).

cence creating new extended defects. The coalescence and aggregation processes result in formation and growth of microvoids, dislocation loops and – considering solute atoms within the matrix – defect cluster-solute complexes or precipitates. The microstructure evolution appears as a consequence of the continuous competition between defect production and elimination.

A matrix damage comprised by various agglomerates of intrinsic point defects and mixed defect-solute agglomerates and by precipitates, typically ≤ 5 nm in size, induces the radiation hardening/embrittlement to RPV steels. In addition, the specific impurity (mainly phosphorus) segregation processes can be found at the precipitate–matrix interface or at grain boundaries. The last process creates a non-matrix component of radiation damage structure and associated embrittlement.

2. Experimental

2.1. Materials

Several types of low-alloy steels used in RPVs have been investigated. These include:

- the base metal and the weld metal of the Cr–Mo–V steel coming from the surveillance material for the VVER-440/213 light-water reactor,

- the IAEA reference steel JRQ of ASTM A533-B Cl.1 type,
- the base metal of the Cr–Ni–Mo–V steel used in the VVER-1000 reactors,
- the base metal of the Cr–Ni–Mo–V steel alloyed additionally with copper or phosphorus.

The list of investigated materials is given in Table 1, their chemical composition and specimen notation are shown in Table 2.

The heat treatment of these materials generally consists of: quenching, tempering and stress relieving. The details of the thermal treatment are given in Table 3.

2.2. Neutron Irradiation

The base metal and the weld metal of the Cr–Mo–V steel were irradiated in surveillance positions of the power reactor VVER-440, the base metal specimen was irradiated also in the research reactor. All other materials were irradiated in the research reactor only.

The surveillance samples were put in vertical channels welded to the outer surface of the core barrel of the VVER-440 reactor on the nuclear power plant. The lead factor was high because of the small thickness of a water reflector in VVER-440 reactors, amounting approximately the value 13 and 18 for the base and the weld metal, respectively. The irradiation temperature ≈ 275 °C was considered to be ≈ 10 °C above that of the inlet water. The aging temperature was 295 °C.

Table 1
Materials

Classification	Steel	Reactor
15Kh2MFA	Cr–Mo–V steel, base metal	VVER-440
Sv-10KhFMT	Cr–Mo–V steel, weld metal	VVER-440
A533-B Cl.1 – JRQ	Plate steel, base metal	PWR of the western type
15Kh2NMFA	Cr–Ni–Mo–V steel, base metal	VVER-1000
15Kh2NMFA alloyed with Cu	Cr–Ni–Mo–V steel, base metal, + Cu	Experimental alloy
15Kh2NMFA alloyed with P	Cr–Ni–Mo–V steel, base metal, + P	Experimental alloy

Table 2
Chemical composition (wt%)

Steel	Specimens	C	Si	Mn	S	P	Cr	Ni	Mo	V	Cu
Cr–Mo–V steel, base metal	A0–A13	0.16	0.17	0.46	0.016	0.014	2.90	0.07	0.66	0.31	0.07
Cr–Mo–V steel, weld metal	B0–B9	0.037	0.59	1.1	0.017	0.012	1.37	–	0.50	0.20	0.06
A533-B Cl.1 plate steel, base metal	C0, C1	0.019	0.25	1.40	0.004	0.019	0.12	0.84	0.50	0.003	0.14
Cr–Ni–Mo–V steel, base metal	D0, D1, D2	0.16	0.26	0.59	0.012	0.005	2.22	1.27	0.63	0.09	0.03
Cr–Ni–Mo–V steel, base metal, + Cu	E0, E1	0.15	0.17	0.48	0.010	0.012	2.06	1.28	0.56	0.10	0.30
Cr–Ni–Mo–V steel, base metal, + P	F0, F1	0.16	0.20	0.34	0.009	0.021	2.14	1.27	0.58	0.10	0.08

Note: Material A – As: 0.008, Co: 0.009, N: 0.0084, O: 0.0039.
Material B – N: 0.0181, O: 0.0813.
Material C – Sol. Al: 0.012.

Table 3
Heat treatment

Material	Processing	Normalization and quenching temperature/time (°C/h)	Tempering temperature/time (°C/h)	Stress relieving temperature/time (°C/h)
15Kh2MFA	Melting, forging	1000/oil 125 °C	690/18	Multiple annealing 680/6, 6, 11, 10.5
Sv-10KhMFT	Welding	–	670/5.5	670/18/furnace
A533-B Cl.1	Melting, rolling	900 °C, quenched 880 °C	665/12	620/40
15Kh2NMFA	Melting, forging	960/6/air + 920/6/water	650/18/air	620/20 + 650/10/furnace
15Kh2NMFA (Cu)	Re-melting and alloying	Homogenization 1200/10, forging at 1180–950 °C	920/20/air	650/10/air + 620/25 + 650/20/furnace to 300 °C
15Kh2NMFA (P)	Re-melting and alloying	Homogenization 1200/10, forging at 1180–950 °C	920/2/air	650/10/air + 620/25 + 650/20/furnace to 300 °C

The samples irradiated in the light water research reactor LVR-15 (or its forerunner VVR-S) were put in an inert gas-filled capsule and placed in the Chouca-rig. The irradiation temperature (275–300 °C) was measured by thermocouples attached to the rig.

Average neutron fluxes and fluences ($E > 0.5$ MeV) for the investigated specimens are given in Table 4.

2.3. Sample preparation

Specimens for TEM and PAS were prepared from samples cut from broken Charpy-V specimens by mechanical grinding and polishing. Thin foils were made using a twin-jet electropolisher at low temperatures. All the specimens for PAS (both PL and DB) were shaped as discs, 8 mm in diameter and 0.25 mm thick. The specimen surfaces were carefully mechanically ground and polished and finally chemically–mechanically polished to minimise the preparation-induced stresses. On the basis of test PL measurements, the fraction of positrons affected by the surface treatment procedure has been estimated [5,6] to be <1%, i.e. reasonably small.

2.4. Transmission electron microscopy

The Tesla BS-540 and JEM 200-CX conventional transmission electron microscopes operated at 120 and 200 kV, respectively, were used for the investigation, allowing for a resolution of ≈ 2 nm for studied (ferromagnetic) materials. The two-beam bright-field and dark-field techniques were applied to the study of radiation-induced defects, dislocation substructures and precipitate particles. The dislocation number density and number density and size of particles and radiation-induced defects were determined by stereological methods using the conventional thickness of a thin foil. That was an average of thickness calculated by counting the number of thickness fringes from a series of micrographs.

2.5. Positron annihilation spectrometers

The PL spectra of the non-irradiated steels were measured by means of BaF₂ lifetime spectrometer [7] providing the timing resolution of 150 ps full width height maximum (FWHM) for ²²Na positron source. The source (~ 1.3 MBq of ²²Na sealed between the two mylar foils of 2 μ m thickness) was sandwiched between the two discs of the studied steel. At least 10⁷ counts were collected in each spectrum. Contribution of positrons annihilating in the source and the covering foils was determined using reference PL measurements with a well-recrystallized α -iron sample. Measured spectra were decomposed into exponential components by means of a procedure described in Ref. [8].

The samples of irradiated steels contained up to 4 MBq of ⁶⁰Co, which emits simultaneously two photons with energies of 1174 and 1332 keV. It causes a significant distortion of measured PL spectrum. Therefore PL spectra of the irradiated steels were measured using the three-detector setup [9] where only triple coincidences belonging to ²²Na (1274 keV start photon plus two annihilation photons 511 keV) are accepted. The spectrometer provides timing resolution of 210 ps FWHM and suppression of the ratio of ⁶⁰Co prompt to ²²Na by a factor of 200 with respect to the standard two-detector mode.

The DB spectra were measured with a high-purity Ge detector (EG&G Ortec) having the energy resolution of 1.9 keV and the peak-to-Compton ratio of 68:1 for 1.33 MeV γ -ray energy. Worsening of the energy resolution of the DB spectrometer occurs with increasing total load. To avoid this effect, a multisandwich composed of reference α -iron sample, RPV steel and a positron source was used as shown in Fig. 1. Firstly, the S -parameter S_{Fe} of α -iron sample was measured in arrangement (a) of Fig. 1. Secondly, the S -parameter S_{RPV} of RPV steel specimen was determined in arrangement (b) of Fig. 1. About 10⁷ counts in the annihilation peak were collected in each run. Relative difference $\Delta S/S_0 = (S_{RPV} - S_{Fe})/S_{Fe}$ which

Table 4
Neutron fluxes and fluences ($E > 0.5$ MeV)^a, irradiation conditions

Specimen notation	Steel	Irradiation time (year)	Neutron flux ($E > 0.5$ MeV) ($\times 10^{16}$ m ⁻² s ⁻¹)	Neutron fluence ($E > 0.5$ MeV) ($\times 10^{24}$ m ⁻²)	Specimen history
A0	15Kh2MFA	–	–	–	Original, non-irradiated
A1	15Kh2MFA	1	3.66	1.12	Irradiated
A3	15Kh2MFA	2	3.89	2.13	Irradiated
A4	15Kh2MFA	3	4.18	3.32	Irradiated
A6	15Kh2MFA	5	4.56	5.89	Irradiated
A7	15Kh2MFA	10	3.83	9.96	Irradiated
A8	15Kh2MFA	5	1.09	1.41	Irradiated and annealed 475 °C/165 h
A10	15Kh2MFA	–	–	–	Thermally aged 295 °C/5 years
A11	15Kh2MFA	–	–	–	Thermally aged 295 °C/10 years
A12	15Kh2MFA	5	1.16	1.79	Irradiated
A13	15Kh2MFA	0.03	57	0.56	Irradiated LVR 15
B0	Sv-10KhMFT	–	–	–	Original, non-irradiated
B2	Sv-10KhMFT	1	4.17	1.22	Irradiated
B3	Sv-10KhMFT	2	4.08	2.20	Irradiated
B4	Sv-10KhMFT	3	4.95	4.02	Irradiated
B6	Sv-10KhMFT	5	3.87	5.26	Irradiated
B7	Sv-10KhMFT	5	2.19	2.97	Irradiated
B8	Sv-10KhMFT	5	3.52	4.78	Irradiated and annealed 475 °C/165 h
B9	Sv-10KhMFT	–	–	–	Thermally aged 295 °C/5 years
C0	A533-B	–	–	–	Original, non-irradiated
C1	A533-B	0.03	57	0.6	Irradiated LVR 15
D0	15Kh2NMFA	–	–	–	Original, non-irradiated
D1	15Kh2NMFA	0.03	29.5	0.29	Irradiated LVR 15
D2	15Kh2NMFA	0.09	34	0.97	Irradiated LVR 15
E0	15Kh2NMFA, Cu	–	–	–	Original, non-irradiated
E1	15Kh2NMFA, Cu	0.02	26	0.15	Irradiated VVR-S
F0	15Kh2NMFA, P	–	–	–	Original, non-irradiated
F1	15Kh2NMFA, P	0.022	26	0.18	Irradiated VVR-S

^aThe coefficient allowing to convert neutron fluences for $E > 1$ MeV is 0.6 for irradiation in the power reactor and the LVR-15 reactor and 0.45 for the VVR-S reactor.

is insensitive to the total load of the spectrometer was used for a measure of irradiation induced defects.

3. Results and discussion

3.1. Transmission electron microscopy

3.1.1. Initial, non-irradiated state

The tempered bainitic–ferritic microstructures are typical for all the materials under the study.

There is only a minor morphological difference among base metal microstructures of specific steel. These microstructures can be classified as the mixture of granular and lath bainite (Fig. 2) with a small amount

of ferrite. The evolution of the microstructure during tempering masks original bainite lath-like morphology, which is seen only infrequently.

The carbide particles precipitating in VVER-type steels differ from those in the A533-B steel. In the former case, blocky chromium-rich carbides of M_7C_3 and $M_{23}C_6$, typically ≈ 0.2 μm in size, precipitate preferably along boundaries. These are accompanied by fine plate-like VC carbides, < 20 nm in size, precipitates more or less homogeneously within the microstructure and in some boundaries. In the later case, the large particles are M_3C -type and small ones are Mo_2C .

The weld metal microstructure of the Cr–Mo–V steel consists predominantly of acicular ferrite in addition to small bainitic areas and network of polyhedral

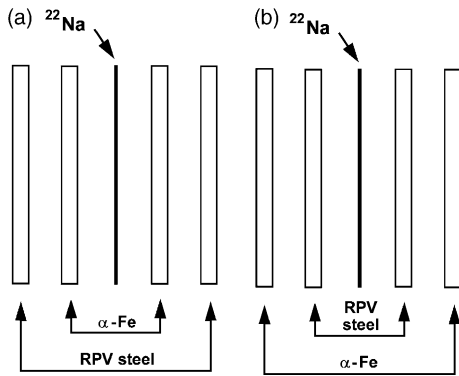


Fig. 1. The two arrangements (a,b) of multisandwich of reference α -iron sample, RPV sample and ^{22}Na source used in DB measurements with purpose to compensate different total load of spectrometer. Explanation is given in text.

proeutectoid ferrite. Precipitates are of same type as in the base metal. The VC carbides are easily observed due to higher vanadium content and lower dislocation density in the weld metal. Microstructures of the base metal

and the weld metal in the as-received state are described in more detail in [10].

The dislocation density in all the materials varies markedly area by area. The average measured dislocation number densities vary from $\approx 1.5 \times 10^{14}$ to $3.5 \times 10^{14} \text{ m}^{-2}$, the lowest values being found in the Cr–Mo–V steel weld metal, Table 5. Typical dislocation substructures allowing for radiation-induced defect investigation are shown in Fig. 3.

3.1.2. Effect of neutron fluence to surveillance specimens

The population of radiation-induced defects found by TEM in both the base metal and the weld metal of Cr–Mo–V-type steel surveillance specimens is identical. It consists of:

- black dots,
- dislocation loops,
- small precipitates.

No microvoids were found in any surveillance specimen investigated by TEM.

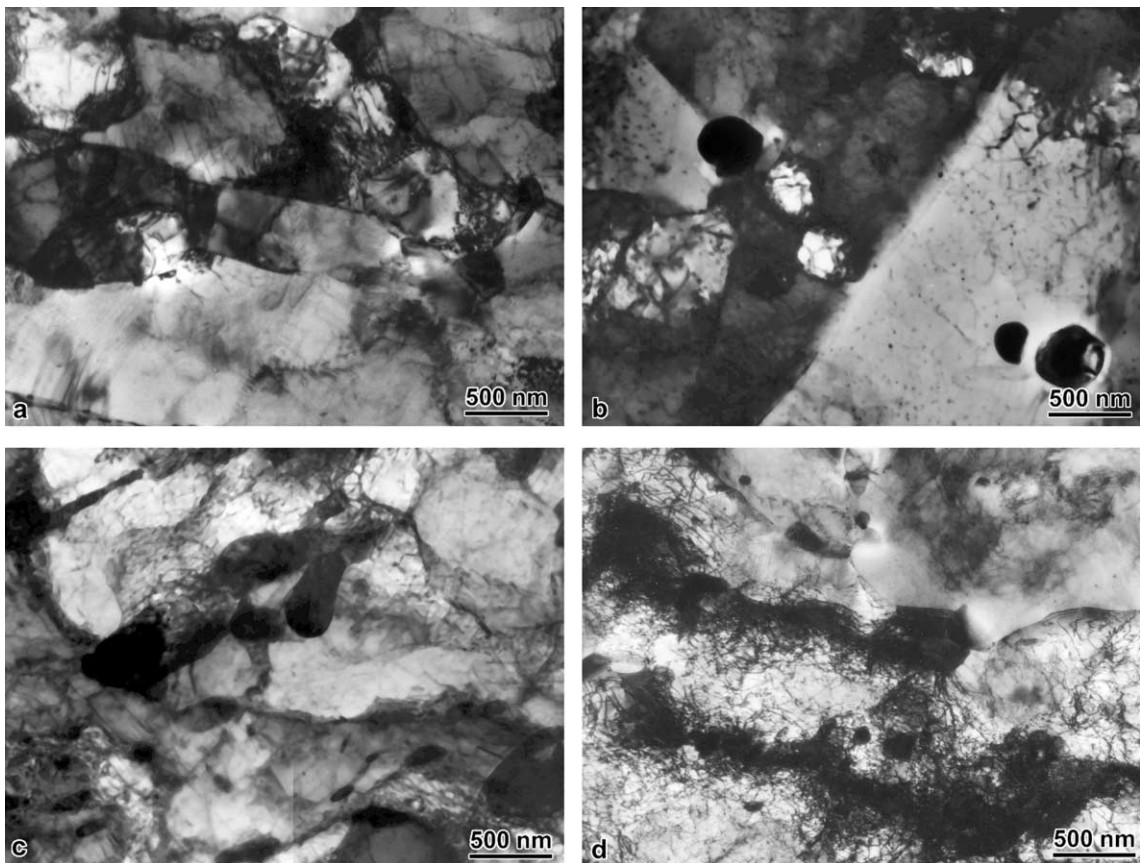


Fig. 2. Microstructures in the as-received materials: the Cr–Mo–V steel, base metal (a), the weld metal (b), JQR A533-B-type steel (c) and the Cr–Ni–Mo–V steel (d).

Table 5
Dislocation number density in as-received materials (the base metals)

Specimen notation	Steel	Dislocation number density ($\times 10^{14} \text{ m}^{-2}$)	Standard deviation ($\times 10^{14} \text{ m}^{-2}$)
A0	15Kh2MFA	2.3	–
B0	Sv-10KhMFT	1.5	0.9
C0	A533-B Cl.1 – JRQ	1.7	0.1
D0	15Kh2NMFA	2.9	1.0
E0	15Kh2NMFA, Cu	3.1	0.5
F0	15Kh2NMFA, P	3.5	1.3

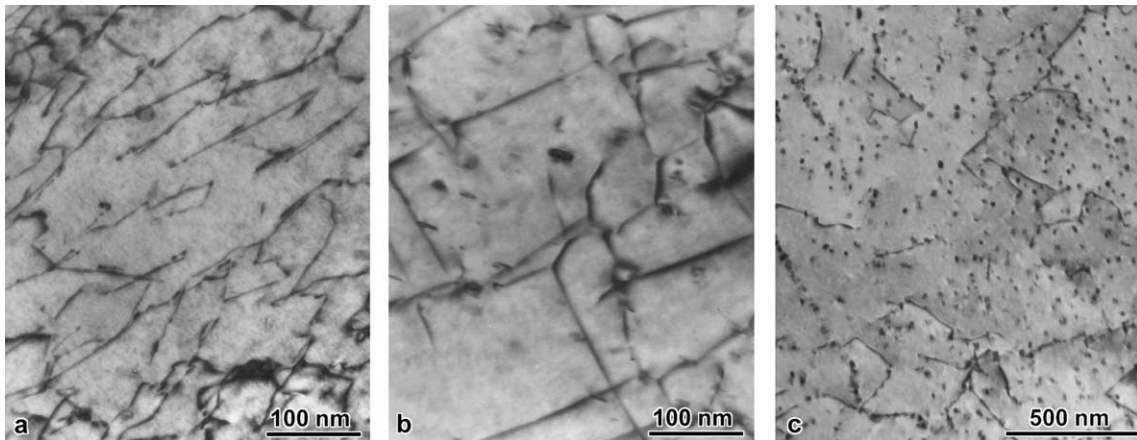


Fig. 3. Characteristic dislocation substructures in the as-received of the Cr–Mo–V steel; bainite in the base metal (a), bainite in the weld metal (b) and pro-eutectoid ferrite in the weld metal (c).

The radiation damage structure of the base metal was described in [6]. As the microstructure of the weld metal is more convenient to perform electron microscopic observations (initial dislocation substructure is more simple, VC particles are easily observed), the quantitative characteristics of radiation-induced defects were evaluated systematically for the weld metal.

Single black dots within a matrix and black dots coalesced near dislocation lines appear after 1 year of neutron exposure of the weld metal specimen in the VVER surveillance position (Fig. 4(a)). With increasing neutron fluence after 3 and 5-year irradiation defect number density as well as their size grow slowly to saturation at about $\approx 1.4 \times 10^{21} \text{ m}^{-2}$ and $\approx 11 \text{ nm}$, respectively (Figs. 5 and 6). Simultaneously, some contrast typical of small dislocation loops and/or precipitates becomes visible and also the tendency of defects to form defect clouds or atmospheres along the length of decorated dislocation lines can be indicated, Fig. 4(b)–(d). The longer the irradiation, the more clearly revealed become the loops and particles, i.e. after 10-year exposition in the base metal, even when density of defects becomes fairly high (Fig. 7).

Similarly, in the base metal the density of defects is growing from $\approx 1.6 \times 10^{21}$ to $\approx 1.9 \times 10^{22} \text{ m}^{-2}$ and the

defect size increasing from ≈ 3 to $\approx 10 \text{ nm}$ for 1 and 10-year irradiation, respectively [6]. These values correspond with results published earlier [11], and are consistent with results published for surveillance specimens as well as templates taken from the VVER-440 power plant reactors [12,13].

The change in the size distribution of VC particles in the weld metal after 5-year irradiation is shown in Fig. 8 in comparison to the non-irradiated and aged specimens. The second peak appearing for the smallest class size (2 nm) can demonstrate the radiation-induced refinement of VC particles due to precipitation of a new population of VC particles.

The nature of the radiation-induced defects was not determined experimentally. It has been already known that the determination of the nature of small radiation-induced clusters ($\leq 5 \text{ nm}$) in TEM is difficult [14]. Further, in tempered bainitic microstructures the heterogeneity of the as-received microstructure resulted from the uneven recovery and polygonization of dislocation substructure is the other factor complicating the evaluation. Finally, small and medium size dislocation loops and small VC precipitates already occurring in the initial microstructure as a result of steel processing can match to radiation-induced defects [10]. In spite of the fact that

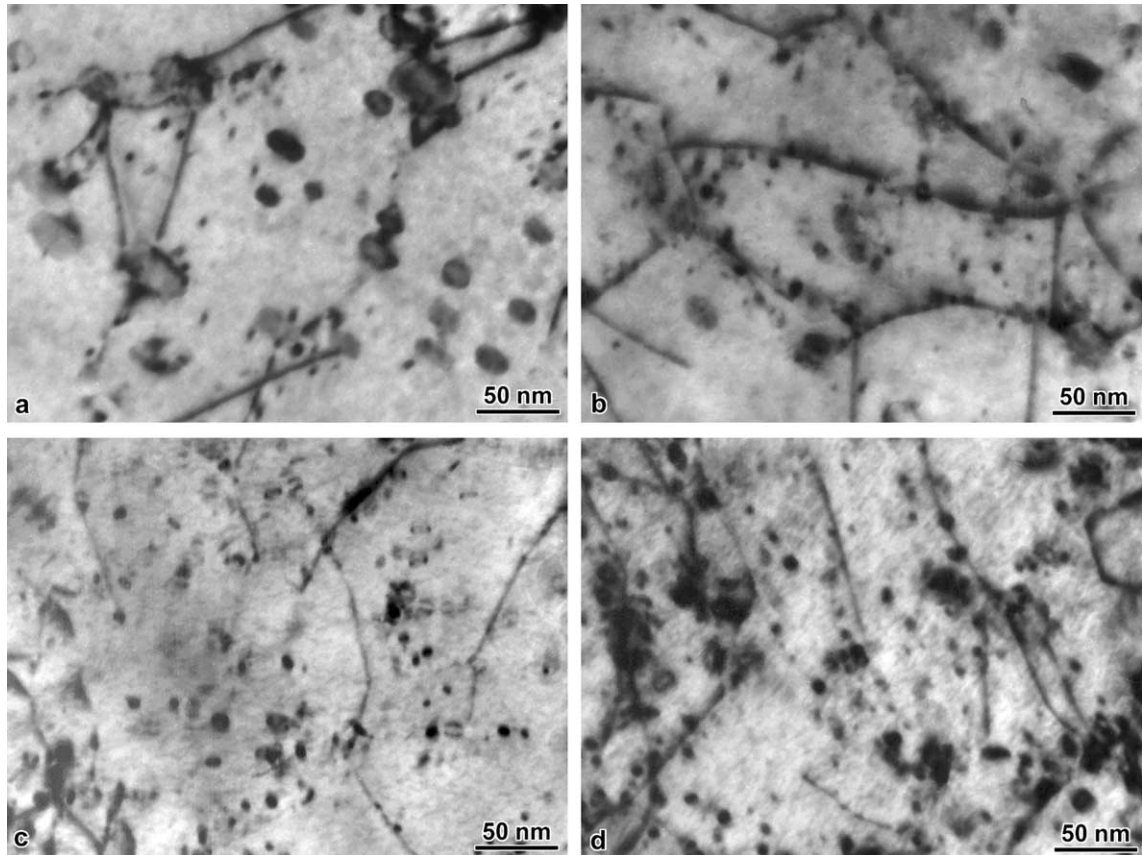


Fig. 4. Microstructure of the weld metal surveillance specimens irradiated to various neutron fluences: $1.22 \times 10^{24} \text{ m}^{-2}$, 1 year irradiated, specimen B2 (a); $2.2 \times 10^{24} \text{ m}^{-2}$, 2 years irradiated, specimen B3 (b); $4 \times 10^{24} \text{ m}^{-2}$, 3 years irradiated, specimen B4 (c) and $5.26 \times 10^{24} \text{ m}^{-2}$, 5 years irradiated, specimen B6 (d).

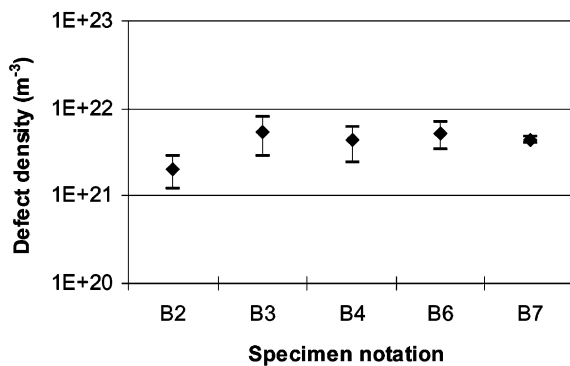


Fig. 5. Number density of radiation-induced defects in the weld metal surveillance specimens. Specimen notation: B2, B3, B4 and B6 – irradiated for 1, 2, 3 and 5 years, respectively; B7 – irradiated for 5 years in a lower neutron flux position.

the analysis of the defects nature failed, there are generally acceptable reasons to assume that complex point defect clusters in addition to dislocation loops and small

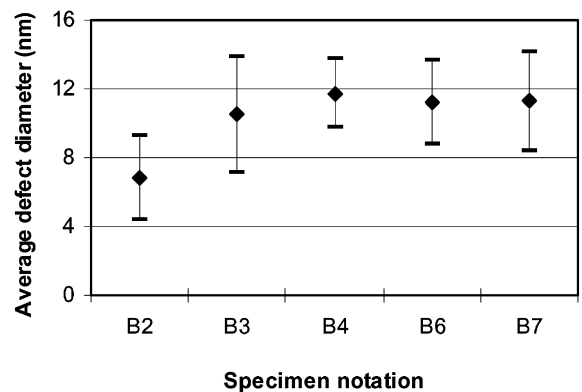


Fig. 6. Size of radiation-induced defects in the weld metal surveillance specimens. Specimen notation: B2, B3, B4 and B6 – irradiated for 1, 2, 3 and 5 years, respectively; B7 – irradiated for 5 years in a lower neutron flux position.

precipitates occur in the radiation-induced population of defects.

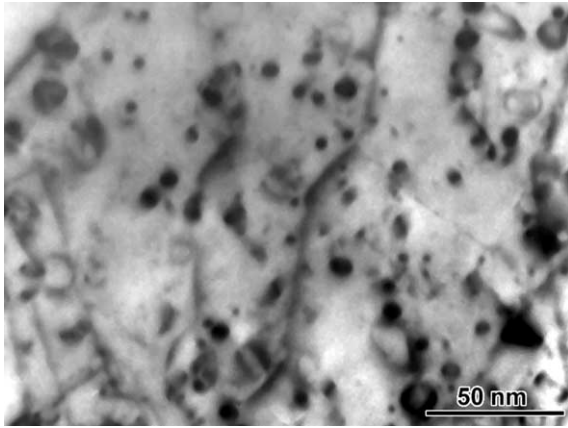


Fig. 7. Microstructure of the Cr–Mo–V steel base metal irradiated for 10 years.

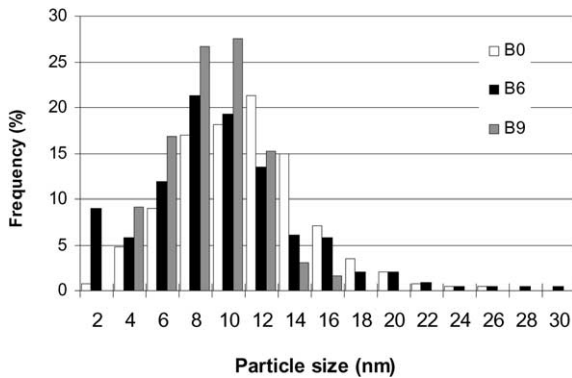


Fig. 8. Size distribution of VC precipitates in the weld metal surveillance specimens. Specimen notation: B0 – non-irradiated; B6 – irradiated for 5 years; B9 – 5 years aged.

Decoration of original dislocations with radiation-induced defects is rather general phenomena in neutron-irradiated materials. According to [15], the decoration of

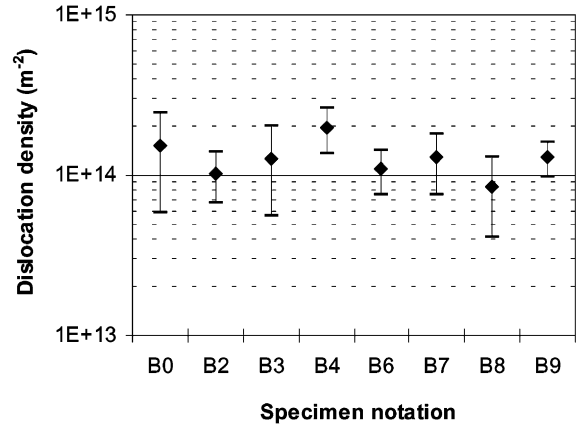


Fig. 9. Dislocation number density measured in thin foils of the Cr–Mo–V steel weld metal. Specimen notation: B0 – non-irradiated; B2, B3, B4 and B6 – irradiated for 1, 2, 3 and 5 years, respectively; B7 – irradiated for 5 years in low neutron flux; B8 – post-irradiation annealed after 5 years irradiation; B9 – 5 years aged.

dislocations by self-interstitial atom (SIA) loops is considered to be due to the trapping of glissile loops rather than migration and successive agglomeration of single SIAs in the strain field of dislocation. Decoration of dislocations with a defect population probably plays a key role in radiation hardening.

The dislocation number density remains nearly unchanged during the irradiation (Table 6 and Fig. 9). Dislocations in highly irradiated specimens of the base metal frequently show bowed segments indicating that climb processes take part in an evolution of dislocation substructure under irradiation.

3.1.3. Neutron flux

Two specimens of the base and weld metal irradiated in (relative) higher and lower neutron flux positions (see Table 4, specimens A6 and A12 and B6 and B7, respectively) were selected from surveillance chains irradiated

Table 6

Dislocation number density in the weld metal after neutron irradiation, post-irradiation annealing and ageing

Specimen notation	Neutron fluence ($E > 0.5$ MeV) ($\times 10^{24}$ m ⁻²)	Neutron flux ($E > 0.5$ MeV) ($\times 10^{16}$ m ⁻² s ⁻¹)	Dislocation number density ($\times 10^{14}$ m ⁻²)	Standard deviation ($\times 10^{14}$ m ⁻²)
B0	–	–	1.5	0.9
B2	1.22	4.17	1.0	0.4
B3	2.20	4.08	1.3	0.7
B4	4.02	4.95	2.0	0.6
B6	5.26	3.87	1.1	0.3
B7	2.97	2.19	1.3	0.5
B8 ^a	3.52	4.78	0.8	0.4
B9 ^b	–	–	1.3	0.3

^a B8 – annealed 475 °C/165 h.

^b B9 – thermally aged at 295 °C/5 years.

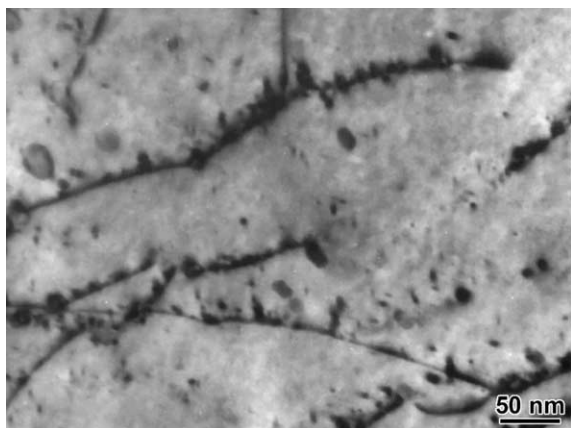


Fig. 10. Microstructure of the weld metal surveillance specimen B7 irradiated to neutron fluence $2.97 \times 10^{24} \text{ m}^{-2}$ in a lower flux position.

for 5 years to assess the neutron flux effect on the microstructure evolution. While black dots, loops and precipitates were found at the higher flux position; only black dot type defects were found in the lower flux position (Fig. 10) in both materials. The amount and distribution of black dots corresponds approximately with 1 and 2-year irradiation at higher flux position.

Similar to the previous investigations [11], no discernible defects appeared after irradiation in the LVR-15 research reactor (irradiated for a short time in one order of magnitude higher neutron flux) in both the VVER type steels and the IAEA A533-B steel irradiated to the neutron fluence $\approx 3 \times 10^{23} \text{ m}^{-2}$ (Fig. 11(a) and (b)). The only exception was the 15Kh2NMFA steel additionally alloyed with 0.3 wt% of copper. In this case, the black dots and probably also the infrequently found

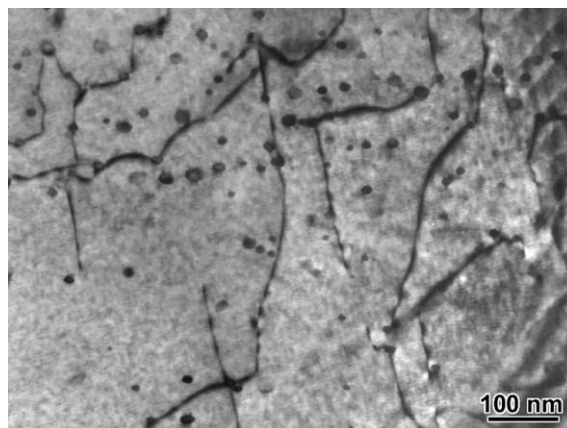


Fig. 12. Microstructure of the weld metal of the B8 surveillance specimen after post-irradiation annealing $475 \text{ °C}/168 \text{ h}$.

groups of precipitates with dislocations may correspond to the copper-enriched precipitates (Fig. 11(c)).

3.1.4. Post-irradiation annealing

Defects present in surveillance materials of the base metal after 5 and 10-year irradiation and the weld metal after 5 year irradiation, disappeared completely during the $475 \text{ °C}/165 \text{ h}$ post irradiation annealing, commonly used for the regeneration of the VVER-440 type RPVs (Fig. 12). Simultaneously, the evident recovery of dislocation substructure occurs (Table 6).

3.1.5. Ageing

No defects resembling radiation-induced defects were seen in the base metal aged for 5 and 10 years and the weld metal aged for 5 years at the operation temperature in the surveillance channel at a position above the

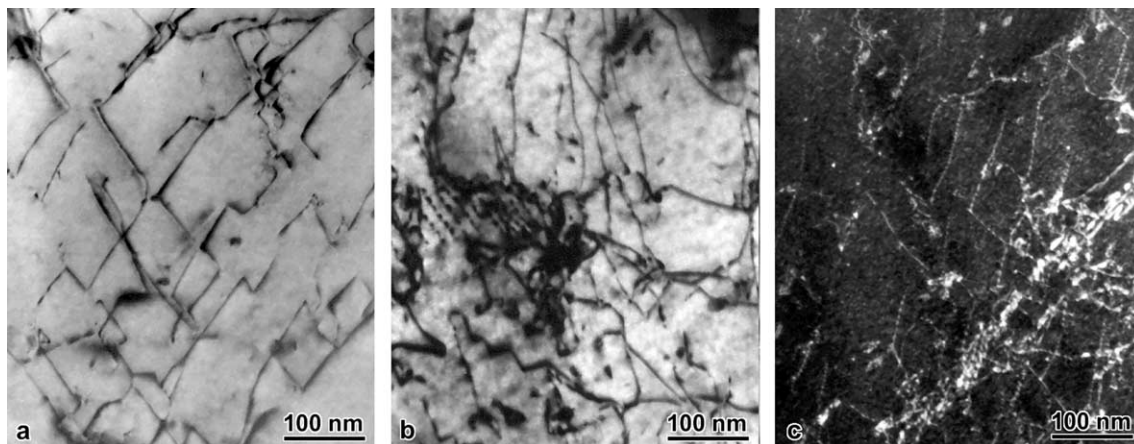


Fig. 11. Microstructure of the neutron irradiated base metal of various 15Kh2NMFA steels: 15Kh2NMFA steel, neutron fluence $0.97 \times 10^{24} \text{ m}^{-2}$, specimen D2 (a); 15Kh2NMFA steel alloyed with 0.021 P, neutron fluence $0.18 \times 10^{24} \text{ m}^{-2}$, specimen F1 (b) and 15Kh2NMFA steel alloyed with 0.3 Cu, neutron fluence $0.15 \times 10^{24} \text{ m}^{-2}$, specimen E1 (c).

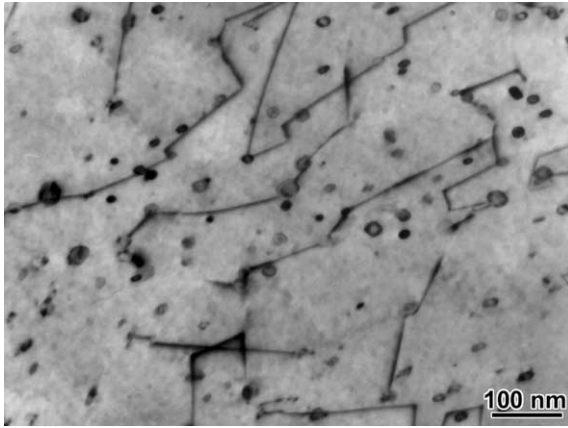


Fig. 13. Microstructure of the weld metal surveillance specimen B9 aged for 5 years at 265 °C.

reactor core (in negligible neutron flux). However, some polygonization of the dislocation substructure was evident (Fig. 13 and Table 6). Only very small coarsening of VC carbides was found (Fig. 8).

3.2. Positron annihilation spectroscopy

3.2.1. Initial, non-irradiated state

Detailed PAS results of study of the non-irradiated RPV steels and extended discussion of these results have been published elsewhere [5]. Therefore, only a brief summary is given here:

- Positron trapping was observed in all types of the materials studied. The τ_1 component corresponds to annihilation of free positrons non-localized in defects. Positrons are trapped mainly at dislocations, lifetime of positrons at dislocations being $\tau_2 = 150$ ps. In Cr–Mo–V steels only a small fraction of positrons may be trapped also at misfit defects at VC precipitate–matrix interfaces.
- Experimental PL data cannot be self-consistently interpreted in terms of the standard two-state trapping model [16] due to non-homogeneous spatial distribution of dislocations in the material.
- The modified trapping model, which takes into account non-uniform distribution of dislocations [5], permitted a self-consistent explanation of the data. Combining the present PL and TEM results, the specific trapping rate at dislocations in α -iron could be deduced as $v_{\text{disl}} = 0.3610^{-4} \text{ m}^2/\text{s}$.
- Increased accuracy of the present PL data permitted the separation of contributions of the screw and edge dislocations. In the A533-B steel, a higher ratio of the screw to edge dislocations was found than in the other materials studied.

3.2.2. Effect of irradiation

The PL and DB results obtained for the irradiated steels were collected in the Table 7 and Figs 14–16. Average PLs τ_{av} observed for the irradiated Cr–Mo–V steels (base material and weld metal) are significantly higher than those for the non-irradiated materials (see the upper part in Fig. 14) which can be understood as a clear evidence that irradiation-induced defects are present in the material. When neutron fluence is increasing, τ_{av} is also growing. Hence the role of the irradiation-induced defects is enhanced, too. Such a conclusion is supported also by behaviour of the S -parameter of the base metal of this steel (see the lower part in Fig. 14). The S -parameter is increased in the irradiated state with respect to the non-irradiated one and exhibits a growth at greater fluences.

A more detailed picture can be obtained from decompositions of the PL spectra into the individual components. It has been found in [5], that the τ_2 component corresponds to positron trapping on dislocations. In comparison with the non-irradiated steels, an additional component with lifetime of $\tau_3 \approx 260$ ps is observed in the irradiated specimens. Such a component corresponds to the positron trapping at defects (presumably vacancy clusters) of open volume comparable to ≈ 5 vacancies [17,18]. Evolution of PLs τ_i ($i = 1, 2, 3$) with fluence (see Fig. 15) shows that there was no significant change of τ_2 (dislocations) and τ_3 (clusters) when fluence was increased, i.e. cluster size is not growing in this fluence range. Therefore, $\tau_2 = 150$ and $\tau_3 = 260$ ps were assumed fixed in evaluations of the fluence dependence of the intensities of spectral components. The intensities I_2 and I_3 (see Fig. 16) exhibited a gradual growth when fluence was increased. In the case of the I_3 , this growth may be understood as a result of increasing number of vacancy clusters, while the I_2 may be enhanced due to increasing concentration of the dislocation loops resulting from a collapse of the vacancy clusters.

Comparison of the specimens irradiated approximately to the same neutron fluence, but at different fluxes, suggests that the effect seen by PAS is independent of flux (see Table 7).

In the A533-B steel (specimen C1), the number of the irradiation-induced defects is almost five times lower than in the Cr–Mo–V steel (specimen A13) irradiated under the similar conditions (see Table 7).

Remarkable decrease of relative intensity I_2 of dislocation component was found in the recovery annealed specimen of base metal of Cr–Mo–V RPV steel (specimen A8) compared to the specimen A12 irradiated under similar conditions (see Table 7). Clearly, it is consequence of recovery of dislocation substructure, which was observed also by TEM (see Section 3.1.4). On the other hand more than two times higher intensity I_3 of irradiation-induced vacancy clusters was found in the

Table 7
PLs and intensities of studied materials

Speci- men no- tation	Steel	Neutron fluence ($E > 0.5$ MeV) ($\times 10^{24}$ m $^{-2}$)	Neutron flux ($E > 0.5$ MeV) ($\times 10^{16}$ m $^{-2}$ s $^{-1}$)	τ_1 (ps)	1st dev.	I_1 (%)	1st dev.	τ_2 (ps)	1st dev.	I_2 (%)	1st dev.	τ_3 (ps)	1st dev.	I_3 (%)	1st dev.	τ_{av} (ps)	1st dev.
A0	15Kh2MFA	–	–	64	5	14.10	0.7	151.6	0.8	85.90	0.60	–	–	–	–	139.2	0.90
A1	15Kh2MFA	1.12	3.66	17	3	14.2	0.7	150	0	75.1	0.5	260	0	10.7	0.3	143	1
A3	15Kh2MFA	2.13	3.89	28	3	11.2	0.4	150	0	76.5	0.4	260	0	12.3	0.3	149	1
A4	15Kh2MFA	3.32	4.18	17	3	11.3	0.8	150	0	77.9	0.7	260	0	10.8	0.3	147	2
A6	15Kh2MFA	5.89	4.56	41	3	9.80	0.3	150	0	78.4	0.4	260	0	11.7	0.3	152.1	0.7
A7	15Kh2MFA	9.96	3.83	0	0	0	0	150	0	85.8	0.4	260	0	14.2	0.5	165.6	0.6
A8	15Kh2MFA	1.41	1.09	38	2	16.3	0.3	150	0	59.8	0.5	260	0	24	0.4	158.1	0.8
A10	15Kh2MFA	–	–	52	4	12.7	0.4	150.5	0.6	87.3	0.4	–	–	–	–	138.0	1
A11	15Kh2MFA	–	–	50	5	12.1	0.5	150.1	0.8	87.9	0.4	–	–	–	–	138.0	0.9
A12	15Kh2MFA	1.79	1.16	40	2	15.9	0.7	150	0	74.9	0.5	260	0	9.3	0.2	142.8	0.5
A13	15Kh2MFA	0.56	57	48	3	12.8	0.3	150	0	77.8	0.5	260	0	9.4	0.3	147.3	0.6
B0	Sv-10KhMFT	–	–	71	4	22	2	151	1	78	1	–	–	–	–	133.6	0.9
B2	Sv-10KhMFT	1.22	4.17	33	1	19.6	0.2	150	0	65.7	0.2	260	0	14.7	0.2	143.2	0.4
B3	Sv-10KhMFT	2.20	4.08	38	2	18.3	0.2	150	0	65.3	0.4	260	0	16.4	0.2	147.5	0.5
B4	Sv-10KhMFT	4.02	4.95	48	2	14.4	0.3	150	0	70	0.5	260	0	15.6	0.3	152.3	0.5
B6	Sv-10KhMFT	5.26	3.87	68	3	19.4	0.7	150	0	63	1	260	0	17.3	0.4	153.2	0.5
B7	Sv-10KhMFT	2.97	2.19	52	2	15.1	0.3	150	0	67.7	0.6	260	0	17.2	0.3	154.1	0.5
B8	Sv-10KhMFT	0.03	3.52	43	3	19.9	0.3	150	0	59.5	0	260	0	22	0.3	154.3	0.7
B9	Sv-10KhMFT	–	–	68	3	27	1	148	1	73	1	–	–	–	–	126.4	0.7
C0	A533-B	–	–	77	4	25	2	148	2	75	2	–	–	–	–	130.1	0.8
C1	A533-B	0.6	57	95	9	28	4	150	0	70	5	260	0	2	0.9	137	2
D0	15Kh2NMFA	–	–	54	6	11.7	0.5	150.1	0.7	88.3	0.4	–	–	–	–	139	1
D1	15Kh2NMFA	0.03	29.5	–	–	–	–	150	0	84.9	0.2	260	0	15.1	0.2	166.6	0.2
D2	15Kh2NMFA	0.09	34	–	–	–	–	150	0	81.9	0.3	260	0	18.1	0.3	169.9	0.4
E0	15Kh2NMFA, Cu	–	–	56	7	10.3	0.6	146.7	0.7	89.7	0.5	–	–	–	–	137	1
E1	15Kh2NMFA, Cu	0.2	26	60	10	16	3	150	0	74	2	260	0	11.1	0.9	148	6
F0	15Kh2NMFA, P	–	–	51	5	12.7	0.5	149.6	0.6	87.3	0.4	–	–	–	–	137	1
F1	15Kh2NMFA, P	0.02	26	–	–	–	–	150	0	76.8	0.2	260	0	23.2	0.2	175.5	0.3

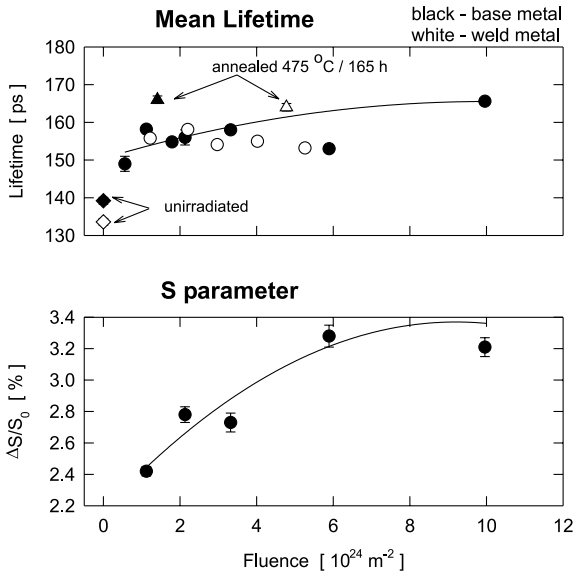


Fig. 14. Dependences of average PL (upper part) and $\Delta S/S_0$ (lower part) on the neutron fluence.

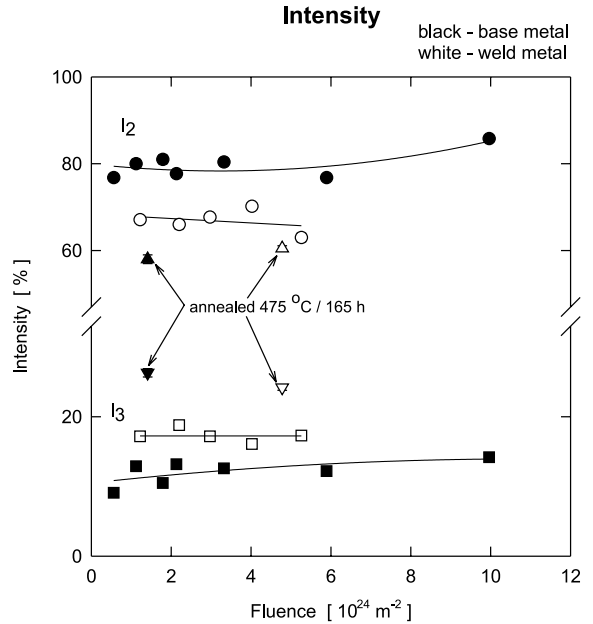


Fig. 16. Intensity of PL components τ_2 and τ_3 in dependence on the neutron fluence.

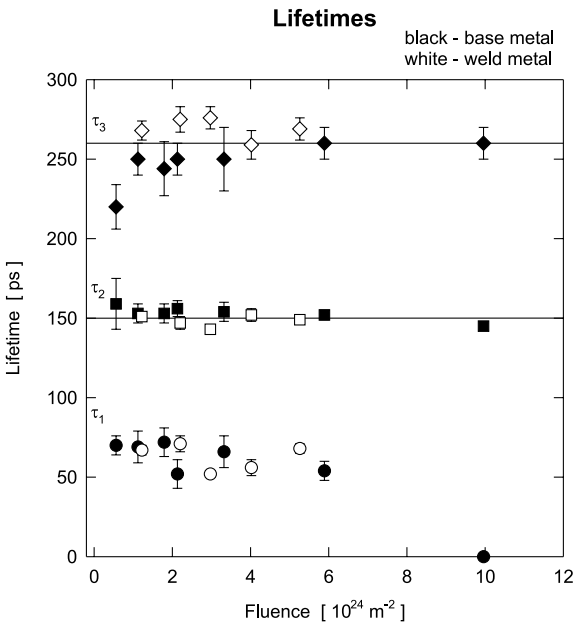


Fig. 15. Decomposition of the PL spectra to individual components in dependence on the neutron fluence.

PL spectrum of specimen A8 compared to A12. This effect of recovery annealing seems to be rather surprising as higher value of I_3 suggests increased number of vacancy clusters in the annealed specimen. As no irradiation-induced defects were observed in present TEM study of the specimen A8, we expect increase of number

of defects, which are below resolution limit of TEM. This increase is also supported by significantly higher value of $\Delta S/S_0 = 4.13 \pm 0.09\%$ for the specimen A8 compared to the values for non-annealed specimens irradiated under similar conditions (see lower panel of Fig. 14). Similar behaviour is exhibited also by weld metal of this steel (specimens B8, B4).

4. Conclusions

Conventional TEM has revealed three kinds of neutron radiation-induced matrix defects in power reactor surveillance specimens. Defect population consists of black dots, small dislocation loops and fine precipitates, concentrated near dislocations and low-angle boundaries. It is believed, that the black dots involve vacancy-solute complexes, in addition to unresolvably small loops and precipitates. No voids were found in TEM.

Only hardly discernible black dots were observed in all the materials irradiated in the research reactor in NRI Řež, except for the 15Kh2NMFA steel additionally alloyed with 0.3 wt% of copper. The black dots observed in this case may correspond to the copper-enriched precipitates.

Dislocation substructure recovery during neutron irradiation of surveillance specimens is very slow. All radiation-induced defects were annealed out during recovery annealing 475 °C/165 h. Simultaneously, a significant recovery of dislocation substructure occurred.

Aging for 10 years at a reactor service temperature results in an advanced polygonization of dislocation substructure and a very small change in VC particles distribution.

PL spectra analysis displayed an additional PL component, amounting 260 ps, in all the materials neutron irradiated in both, power and research reactor. This corresponds to the positron trapping centre of open volume comparable to 5–6 vacancies, i.e. vacancy clusters or microvoids. Occurrence of this type of defect is independent of a neutron flux and neutron fluence, intensity is growing with increasing neutron fluence.

Acknowledgements

Financial support provided by the Grant Agency of the Czech Academy of Sciences under the grant no. 106/96/1319 is gratefully acknowledged.

References

- [1] W.J. Phythian, C.A. English, *J. Nucl. Mater.* 205 (1993) 162.
- [2] D.J. Bacon, T. Diaz de la Rubia, *J. Nucl. Mater.* 216 (1994) 275.
- [3] R.E. Stoller, G.R. Odette, B.D. Wirth, *J. Nucl. Mater.* 251 (1997) 49.
- [4] D.J. Bacon, A.F. Calder, F. Gao, *J. Nucl. Mater.* 251 (1997) 1.
- [5] J. Čížek, I. Procházka, J. Kočík, E. Keilová, *Phys. Status Solid A* 178 (2000) 651.
- [6] J. Kočík, E. Keilová, I. Procházka, J. Čížek, in: M.L. Hamilton, A.S. Kumar, S.T. Rosinski, M.L. Grossbeck (Eds.), *Proceedings of the 19th Symposium on Effects of Radiation on Materials*, Seattle, June 1998, ASTM STP-1366, ASTM, West Conshohocken, PA, 1999, p. 354.
- [7] F. Bečvář, J. Čížek, I. Procházka, *Acta Phys. Polon. A* 95 (1999) 448.
- [8] I. Procházka, I. Novotný, F. Bečvář, *Mater. Sci. Forum* 255–257 (1997) 772.
- [9] J. Čížek, F. Bečvář, I. Procházka, *Nucl. Instrum. and Meth. A* 450 (2000) 325.
- [10] J. Kočík, E. Keilová, *Nucleon* 3 (1998) 19.
- [11] J. Kočík, E. Keilová, in: *Joint IAEA/NEA Specialists' Meeting on Irradiation Embrittlement and Optimisation of Annealing*, Paris, September 1993.
- [12] B.A. Gurovich, E.A. Kuleshova, O.V. Lavrenchuk, K.H. Prikhodko, Ya.I. Strombakh, *J. Nucl. Mater.* 264 (1999) 333.
- [13] I.V. Gorynin, E.V. Nesterova, V.A. Nikolaev, V.V. Rybin, in: D.S. Gelles, R.K. Nanstad, A.S. Kumar, E.A. Little (Eds.), *Proceedings of the 17th International Symposium on Effects of Radiation on Materials*, Sun Valley, June 1994, ASTM STP-1270, ASTM, 1996, p. 248.
- [14] M.L. Jenkins, H. Fukushima, M.A. Kirk, in: I.M. Robertson, G.S. Was, L.W. Hobbs, T. Diaz de la Rubia (Eds.), *Microstructure Evolution During Irradiation*, Symposium Proceedings, Vol. 439, Materials Research Society, Pittsburgh, PA, 1997, p. 289.
- [15] H. Trinkaus, B.N. Singh, A.J.E. Foreman, *J. Nucl. Mater.* 249 (1997) 91.
- [16] P. Hautojärvi, C. Corbel, in: A. Dupasquier, A.P. Millsjr (Eds.), *Positron Spectroscopy of Solids*, Proceedings of International School of Physics 'Enrico Fermi' Course CXXV, IOS, 1995, p. 491.
- [17] M.J. Puska, R.M. Nieminen, *J. Phys. F* 13 (1983) 333.
- [18] A. Hempel, M. Saneyasu, Z. Tang, M. Hasegawa, G. Brauer, F. Plazaola, S. Yamaguchi, in: M.L. Hamilton, A.S. Kumar, S.T. Rosinski, M.L. Grossbeck (Eds.), *Proceedings of the 19th Symposium on Effects of Radiation on Materials*, Seattle, June 1998, ASTM STP-1366, ASTM, West Conshohocken, PA, 1999, p. 560.